Analytical and Bioanalytical Chemistry
https://doi.org/10.1007/s00216-022-04367-y

RESEARCH PAPER

Engineering a thermostable biosensor based on biomimetic mineralization HRP@Fe-MOF for Alzheimer's disease

Yang-Bao Miao[1] · Qilong Zhong[2] · Hong-Xia Ren[3]

Received: 27 June 2022 / Revised: 30 August 2022 / Accepted: 30 September 2022

Abstract

The development of disease detection by biosensors represents one of the key components of medical science. However, millions of people are still misdiagnosed each year due to the poor efficacy and thermal instability of biosensors. Using horseradish peroxidase (HRP) as a paradigm, we offer a rational design strategy to optimize the thermostability and activity of biosensors by biomimetic mineralization. To overcome the weak thermostability of the biosensor, the mineralization of Fe-MOF forms an armor on HRP that protects against high temperature. Additionally, the biomimetic mineralization HRP@Fe-MOF can double-catalyze the TMB/H_2O_2 chromogenic system for color development. The biosensor can also be recycled through simple heat treatment due to the thermally stable aptamer and biomimetic mineralization HRP@Fe-MOF. The optical biosensor based on this sensitive spectral transformation was successfully developed for the measurement of AβO with an outstanding linear range (0.0001–10 nM) and a low limit of detection (LOD) of 0.03 pM. This promising platform will open up new avenues for the detection of AβO in the early diagnosis of Alzheimer's disease (AD).

Keywords Biomimetic mineralization · Strand displacement assay · Optical sensors · Signal amplification · Alzheimer's disease

Introduction

Alzheimer's disease (AD), an emerging affliction of the aging population, is a type of chronic neurodegenerative disease that over time causes debilitating problems with thinking, memory, and behavior [1]. Evidence demonstrates that amyloid-beta oligomers (AβO) play an important role in AD [2]. Accurate identification of AβO levels can improve the accuracy of early diagnosis of AD and the timing of treatment [3]. Many different types of biosensors have recently been developed for the detection of AβO that can be used for this purpose, including fluorescence sensors [4], enzyme-linked immunosorbent assay (ELISA) [5], Raman spectroscopy [6], electrochemical sensors [7], and electrochemiluminescence sensors [8]. A number of different detection assays are available for research; however, the instability and low efficacy of biosensor products lead to a rapid loss of potency during delivery and storage, severely restricting the scope of existing biosensor programs [9].

To address these concerns, a biomimetic mineralization of HRP@Fe-MOF nanoparticles that is resistant to ambient temperature may act synergistically as a catalyst by Fenton reaction. Iron(II) salts are the most commonly used Fenton reagent because Fe(II) is oxidized by hydrogen peroxide (H_2O_2) to the form Fe(III) [10]. As a result, disproportionation of H_2O_2 in the form of a hydroxyl radical (OH) is produced, which promotes color reaction [11]. Metal–organic frameworks (MOFs) are ordered porous materials that are created by combining organic ligands with metal ions to form a desired structure [12–14]. Because of the low toxicity of the Fe-MOF, it has been utilized in a wide variety of research [14]. In the biosensor area, MOFs are generally used as a carrier to combine signal substances, aptamer, or antibody [15–17]. Aptamers, which are single-stranded DNA or RNA oligonucleotides that bind to their targets with

✉ Hong-Xia Ren
renhongxiahappy@126.com

[1] Department of Haematology, Sichuan Academy of Medical Sciences & Sichuan Provincial People's Hospital, School of Medicine of University of Electronic Science and Technology of China, No. 32, West Section 2, First Ring Road, Qingyang District, Chengdu 610000, China

[2] Ningbo No. 7 Hospital, Ningbo 510530, China

[3] School of Chemistry and Chemical Engineering, Zunyi Normal College, Guizhou 563000, China

Published online: 18 October 2022

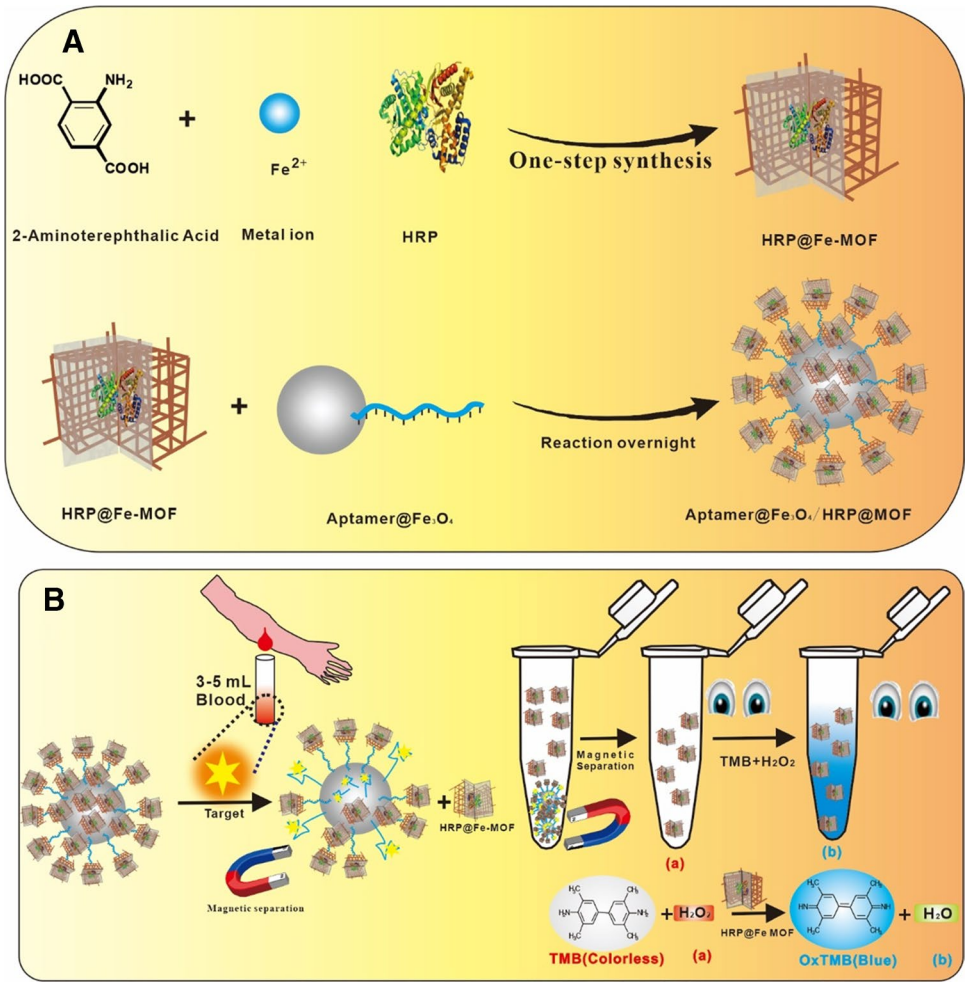

Scheme 1 (**A**) Preparation of the biomimetic mineralization HRP@Fe-MOF and (**B**) the process for monitoring of AβO and optical biosensor

high affinity and specificity, have several advantages over their antibody counterparts, including long-term stability, the ability to be modified, higher binding affinity, pH stability, and limited immunogenicity.

Here, a straightforward one-pot method for the preparation of biomimetic mineralization HRP@Fe-MOF is presented. We protected the horseradish peroxidase (HRP) with an armor shell-like exterior [18], which is self-assembled under mild sonication due to the engineered Fe(II)-based MOF biomineralization catalase. The biomimetic mineralization of Fe(II)-MOF around catalase (HRP@Fe-MOF) forms a strong exoskeletal cage, increasing the encapsulated catalase to improve thermostability.

The development of a biosensor based on biomimetic mineralization HRP@Fe-MOF for AβO detection that is stable, selective, and specific is necessary to effectively detect AβO (Scheme 1). This strategy is developed to increase the sensitivity of detection by using Fe(II)-based MOF armored catalase (HRP@Fe-MOF) as a double-signal amplification tag conjugated capture probe (AβO aptamer-Fe_3O_4). During the process of probe generation, the aptamer chain of the capture probe connects to the Fe-MOF on the signaling probe by electrostatic, π-stacking, and/or hydrogen-bonding interactions. When AβO is present in the blood sample, which can be specifically recognized using this optical biosensor, biomimetic mineralization HRP@Me-MOF is released into the solution using the target-induced strand displacement assay [19]. This occurs primarily because the binding ability of the target to the aptamer is greater than that of the aptamer and MOF. The biomimetic mineralization HRP@Fe-MOF that is released can double-amplify the chromogenic signal of TMB/H_2O_2. Also, at room temperature, the aptamer in the capture probe, which is reconstituted from the AβO/Apt-Fe_3O complex through heat treatment, can bind to HRP@Fe-MOF again by coordinate bonding. The biomineralized engineered biosensor is a novel candidate for the detection of AβO and is worth promotion and reference. Additionally, the cost-effectiveness of this biosensor is appropriate for practical applications.

Experimental

Materials and reagents

2-Aminoterephthalic acid, ferric sulfate, and HRP were obtained from Alfa Aesar (Tewksbury, MA, USA). The aptamer sequence of AβO (5′-COOH-GCCTGTGGTGTT GGGGCGGGTGCG) [19] was synthesized by Sangon Biotech (Shanghai, China, https://www.sangon.com/). Immunoglobulin G (IgG), IgA, oleic acid, Aβ protein fragment 1-42 and lipid were purchased from Sigma-Aldrich (St. Louis, MO, USA). A human AβO ELISA kit was obtained from VWR International (Radnor, PA, USA). All chemicals were of analytical reagent grade.

Synthesis of Apt-Fe_3O_4 complex

The synthesis of colloidal Fe_3O_4 nanoparticles (NPs) was carried out in accordance with a prior publication [20]. First, iron oleate complex (2 mmol) and NaOH (2.5 mmol) were added to 10 mL of ethanol at room temperature to obtain a homogeneous solution. The mixed solution was then transferred into a 100 mL autoclave and heated at 180 °C for 10 hours, after which the system was cooled to room temperature. The oleic acid-coated Fe_3O_4 NPs were obtained by washing three times with hexane. The ligand (amino functionalization) exchange approach used was described previously and is a typical surface modification method for Fe_3O_4 NPs [21].

Conjugation of Apt-Fe_3O_4 (capture probes) was performed by carbodiimide cross-linking [22]. The obtained capture probes were washed four times, and the free-form aptamer was removed via magnet. Finally, the apt-Fe_3O_4 complex was stored at 4 °C before use.

Preparation of signal probe

Biomimetic mineralization HRP@Fe-MOF NPs were synthesized by an ultrasonic synthesis method [18]. The HRP@Fe-MOF NPs were made by dispersing 1.0 mmol of 2-aminoterephthalic acid, 10 M HRP, and 1.0 mmol of $FeSO_4$ in 50 mL of double-distilled (DI) water in a 50 mL Eppendorf tube. The mixture was reacted for 1 hour under 25 °C via sonication. The resulting HRP@Fe-MOF was washed three times with double-distilled water.

To determine the protein loading content (LC) and loading efficiency (LE) in the HRP@Fe-MOF, weighed test samples were dissolved in ethylenediaminetetraacetic acid (EDTA, 0.1 M) and then shaken at room temperature for 3 h in order to release their encapsulated HRP. The amount of released HRP was determined using a Pierce BCA Protein Assay Kit (Thermo Fisher Scientific, Waltham, MA, USA). This information was then utilized to compute the LE and LC of HRP in the HRP@Fe-MOF by employing the formulae provided below.

$$\mathrm{LE}\% = \frac{\text{weight of HRP in HRP@Fe–MOF}}{\text{total amount of HRP added}} \times 100\%$$

$$\mathrm{LC} = \frac{\textit{weight of HRP in } \text{HRP@Fe–MOF}}{\textit{weight of } \text{HRP@Fe–MOF}} \times 100\%$$

Preparation of optical biosensor for AβO detection

The optical biosensor was prepared by combining the reaction products of the capture probe Apt-Fe_3O_4 (10 mg/mL) and signal probe HRP@Fe-MOF (10 mg/mL) overnight. To detect AβO, various concentrations of the AβO sample were added to the optical biosensor solution at 25 °C. After 30 min of processing, magnetic separation was used to obtain the supernatant. After adding 100 L of 1 mM TMB and 1 mM H_2O_2 to the supernatant (100 µL), the color development in the supernatant was visible to the naked eye. Finally, quantitative data at 650 nm was determined using an ultraviolet–visible (UV–Vis) spectrometer.

Blood sample test and reusability of the biosensor

The serum sample used for method development was obtained from leftover specimens in the Department of Laboratory Medicine, Ningbo No. 7 Hospital. The collection of samples was approved by the Ethics Committee of Ningbo No. 7 Hospital. In order to detect AβO, varied amounts of AβO or blood sample were each introduced into an optical biosensor in a volume of 100 µL and allowed to incubate for 30 min at room temperature. Magnetic separation was then utilized to obtain the supernatant. Next, 50 L of supernatant was dosed with 0.01% TMB and 0.015% H_2O_2 so that a color change could be observed with the naked eye. At the completion of the process, the solution was vigorously shaken to encourage color development, and the absorbance was measured using a UV–Vis spectrometer at 650 nm for quantitative analysis.

When the AβO was present in the serum sample, the AβO aptamer in the capture probes could specifically distinguish the AβO. Meanwhile, the signal probe was released into the supernatant for color development. To evaluate the reusability of the biosensor, the materials (HRP@Fe-MOF and (AβO/Apt-Fe_3O_4 complex) were directly collected after testing of the biosensor. The aptamer was then reconstituted from the conjugated AβO of Apt-Fe_3,O_4 by heating at 90 °C for 1 min. The pure nucleic acid aptamers were then obtained by magnetic separation of the multiple products,

and the reconstituted aptamer in Fe_3O_4 NPs once again bound to HRP@Fe-MOF with overnight reaction [23].

Results and discussion

Characterization of biomimetic mineralization HRP@Fe-MOF and capture probe

The biomimetic mineralization HRP@Fe-MOF and Apt-Fe_3O_4 complex nanoparticles exhibit an elongated morphology, as detected using transmission electron microscopy (TEM, Fig. 1a). Dynamic light scattering (DLS, $n = 6$ batches) analysis of the biomimetic mineralization HRP@Fe-MOF depicts an elongated shape, with an average diameter of 22.7 ± 1.8 nm (see Electronic Supplementary Material Fig. S1) and zeta potential of 19.6 ± 3.8 mV (see Electronic Supplementary Material Fig. S2). Powder X-ray diffraction (XRD) data (see Electronic Supplementary Material Fig. S3) confirm the mineralization of Fe-MOFs around the HRP (HRP@Fe-MOF) successfully formed exoskeletal cage, and the structure of the Fe-MOFs is similar to that reported for the MIL-53(Fe) phase [24]. Analysis of the energy-dispersive X-ray spectroscopy (EDS) line scanning profile reveals elemental composition of HRP@Fe-MOF that confirms the successful encapsulation of HRP in the HRP@Fe-MOF (Fig. 1b). After the addition of DI water of HRP@Fe-MOF, the nanoparticles are triggered to a transparent solution (see the Tyndall effect in HRP@Fe-MOF nanoparticle solutions [1] and DI water [2] in Fig. 1c) [25]. The UV–Vis absorption spectra of HRP@Fe-MOF (pink curve), HRP (blue curve), aminated terephthalic acid (red curve), and ferrous sulfate solution (black curve) are revealed in Fig. 1d. The blue curve illustrates that the maximum absorption peak is at 406 nm (the typical peak of HRP) [25]. Moreover, the maximum absorption wavelength of HRP@Fe-MOF NPs is redshifted from 406 nm (the characteristic peak of HRP) to 408 nm for the interaction between HRP@Fe-MOF NPs [26]. The Fourier transform infrared (FT-IR) spectra further reveal that the Fe-MOF-armored HRP did not modify its structural properties from those detected in the original HRP (bands in the ranges of 1640–1660 and 1510–1560 cm^{-1} were amide I and II bands, respectively) (see Electronic Supplementary Material Fig. S4). Figure 1e and f shows TEM images of the capture probe nanostructures and aptasensor. The diameters of the particle are about 100 nm (see Electronic Supplementary Material Fig. S5) and 130 nm (see Electronic Supplementary Material Fig. S6), respectively. Figure 1f clearly illustrates

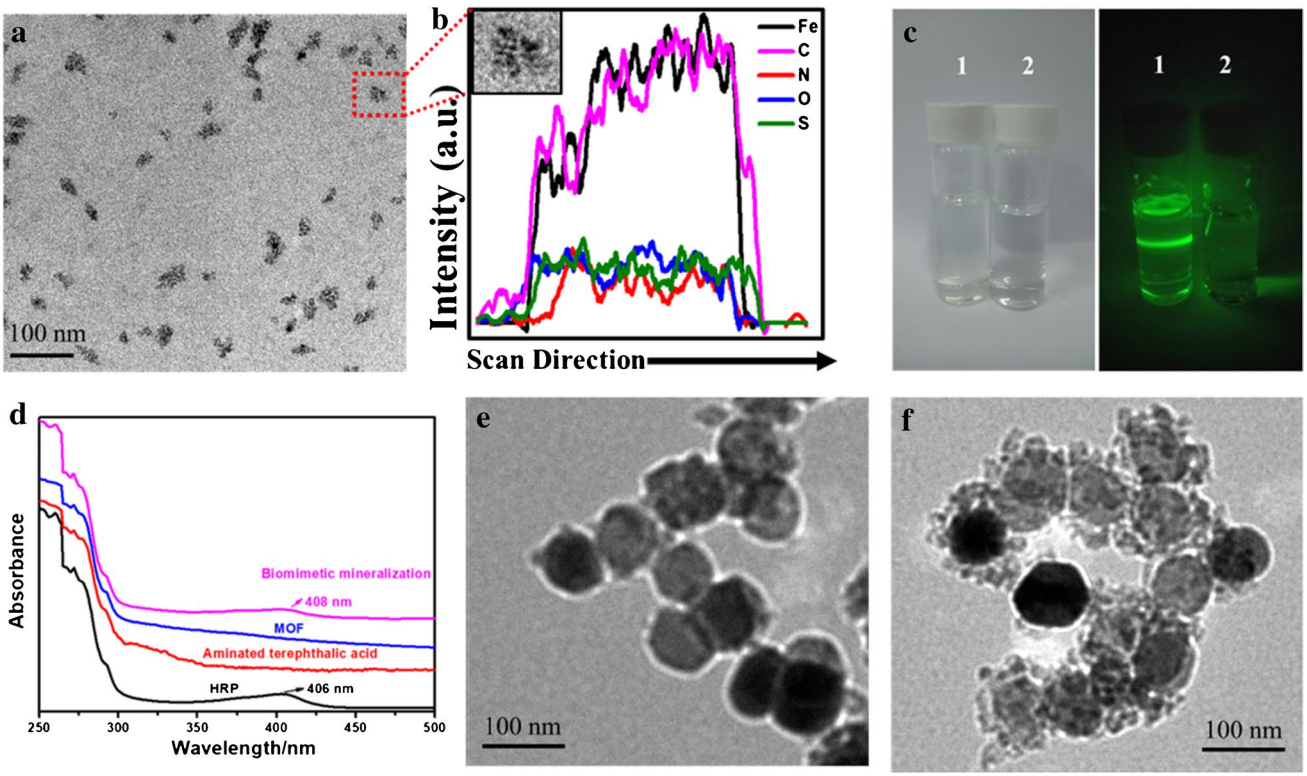

Fig. 1 (**a**) TEM micrograph of HRP@Fe-MOF, (**b**) elemental line scan of HRP@Fe-MOF. (**c**) Photo displays the Tyndall effect in solutions with HRP@Fe-MOF nanoparticle solution (1) and (2) DI water. (**d**) UV–Vis spectra of HRP (black curve), MOF (blue curve), aminated terephthalic acid (red curve), and HRP@Fe-MOF (pink curve) obtained through the related solution. TEM micrograph of aptamer-Fe_3O_4 (**e**) and biosensor (**f**)

that the surface of the capture probe was conjugated with a layer of HRP@Fe-MOF. Overall, the nanoscale biosensor is successfully synthesized.

To maximize the amount of the protein (HRP) that could be loaded on the Fe-MOF by biomimetic mineralization, the formulation of the HRP@Fe-MOF was improved by regulating the feeding concentration ratio of the HRP to the Fe-MOF. As demonstrated in Table S1, as this feeding ratio increased, the protein loading content (LC) in the HRP@Fe-MOF increased and its protein loading efficiency (LE) decreased. However, when the HRP-to-Fe-MOF ratio was increased to 1:1, the protein loading content was greatest. Therefore, the HRP@Fe-MOF that was synthesized at an HRP-to-Fe-MOF ratio of 1:1, which had an LC of 48.3±1.5% and an LE of 93.6±4.2% (n = 6 batches), was employed in the following tests.

The sensor signal amplification strategy and reusability studies

To further confirm the feasibility of the biosensor, the UV–Vis spectrum of the TMB-H_2O_2 solution was detected under various conditions (Fig. 2). The mechanism of TMB with H_2O_2 color development under HRP@Fe-MOF as a signal probe is presented in Fig. 2a. The colorless TMB that was used as the starting substrate with the H_2O_2 was transformed into its blue oxidation state as a result of the catalyst (Fig. 2b). It can be clearly seen that the TMB-H_2O_2 solution (black curve) yielded no color change, while the characteristic peak was observed under Fe-MOFs (100 µg/mL) as signal probe in the biosensor and the TMB-H_2O_2 solution (red curve) at 650 nm. Subsequently, the TMB-H_2O_2 solution produced a dramatic color change at 650 nm when HRP@Fe-MOF (100 µg/mL) was used as signal probe in the biosensor (blue curve). As a result, one may conclude that HRP@Fe-MOF enables an oxidation reaction to occur during double signal amplification.

In nature, biomineral coatings are frequently utilized as a method for protecting soft tissue from the environment in which it is located. Based on this information, we decided to investigate whether MOF coatings may create a comparable barrier that would enable implanted biomacromolecules to endure harsh conditions (such as high temperature) that would ordinarily lead to their breakdown. To verify whether the mineralized Fe-MOFs could maintain the activity of the catalytic enzyme (HRP) at 37 °C for long periods, a TMB/H_2O_2 chromogenic system was applied for enzymatic activity [27]. Figure 2c plots the stability of free-form HRP and Fe-MOFs-armored HRP that had been stored in NaCl (pH=7.0) at 37 °C for 4 weeks. The free-form HRP showed that almost all HRP activity was inactivated within 3 days at 37 °C. However, the Fe-MOF-armored-HRP maintained approximately 90% of its activity after 4 weeks.

Typically, exposing enzymes to elevated temperatures results in an irreversible loss of bioactivity due to the disruption of non-covalent interactions. Thus, we assessed whether an HRP Fe-MOF coating could enhance their stability against extreme conditions. As shown in Electronic Supplementary Material Fig. S7, HRP was protected at 100 °C by the mineralization MOF layer, whereas the free enzyme completely lost activity. These experiments confirm that the MOF coating functions as a protective covering for

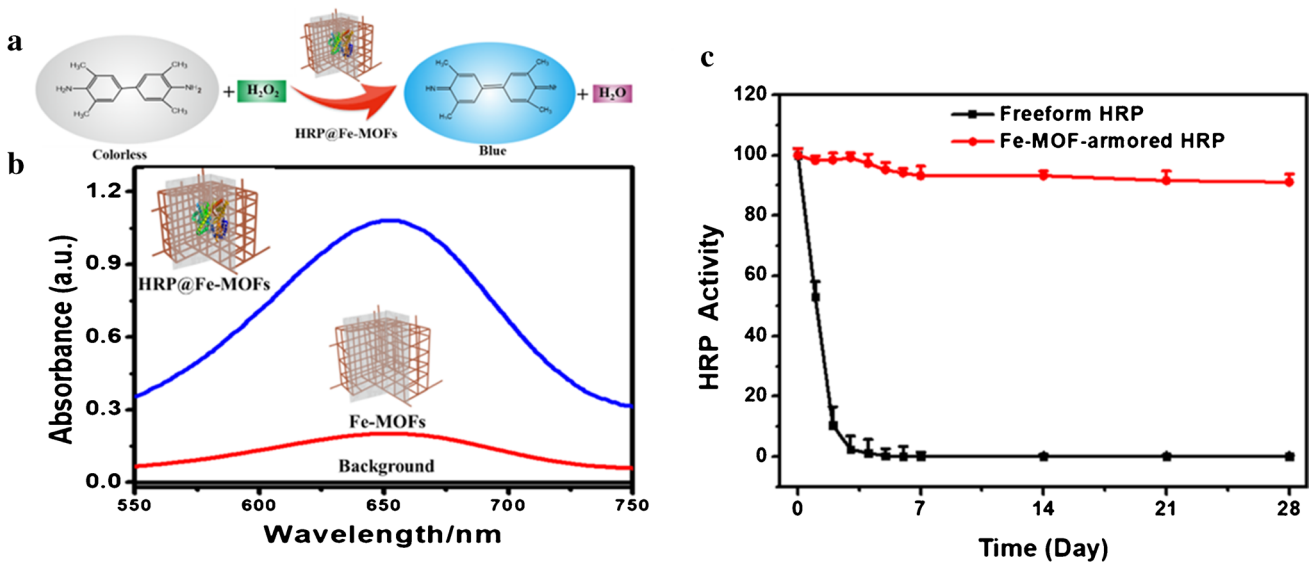

Fig. 2 (**a**) Mechanism tested with the optical biosensor; (**b**) UV–Vis spectra of TMB solution with different signal probes (absence of signal probe, black curve, Fe-MOFs (red curve) and HRP@Fe-MOF (blue curve); (**c**) enzymatic activity of free-form HRP and Fe-MOF-armored HRP after storage in NaCl (pH=7.0) at 37 °C for predetermined intervals

the enzyme at high temperature, while the encapsulated enzymes are still able to communicate with their surrounding environment despite the presence of this protective covering. This is because the pore structure of the Fe-MOF is unchanged before or after the encapsulation of the HRP (see Electronic Supplementary Material Fig. S8). The porous features of Fe-MOF before and after encapsulation of HRP were analyzed using the Brunauer–Emmett–Teller (BET) method. pH stability is a pivotal property of MOFs for their widespread use in solution. Therefore, the stability of Fe-MOF@HRP under the exposure of different pH values was evaluated by DLS (see Electronic Supplementary Material Fig. S9). The results indicate that the material was stable under pH 2–7. This finding suggests that the mineralized Fe-MOF armored enzyme has the benefit of maintaining high activity, which hopefully solves the problem of thermal instability in biosensors.

When AβO encountered the biosensor, the aptamer in the capture probe was able to specifically identify the AβO, after which HRP@Fe-MOF NPs were released into the solution based on displacement strategies (Fig. 3a) [28]. In order to effectively illustrate the probe reproducibility, we conducted a leaching study of HRP@Fe-MOF. As shown in Electronic Supplementary Material Fig. S10, the activity of the HRP protein was not affected by the number of leaching studies. As shown in Fig. 3b, the proposed biosensor was subsequently able to be recycled 10 times with no significant difference in the monitoring signal via heating of the AβO/Apt-Fe_3O_4 NP complex at 90 °C.

Selectivity of the optical biosensor

To assess the selectivity of the optical biosensor, we applied the main components of blood (Na^+, K^+, IgA, BSA, glucose, lipids, and IgG) [29], which were added separately and independently to the physiological saline, meant to simulate blood concentration. As demonstrated in Fig. 4, there is no remarkable difference in the interference introduced with or without the addition of these interference substances. Additionally, there is no UV–Vis absorption signal with only interfering substances in solution, demonstrating that the optical biosensor can successful distinguish AβO. In addition, the principal components do not show any substantial cross-reactivity in the blood samples.

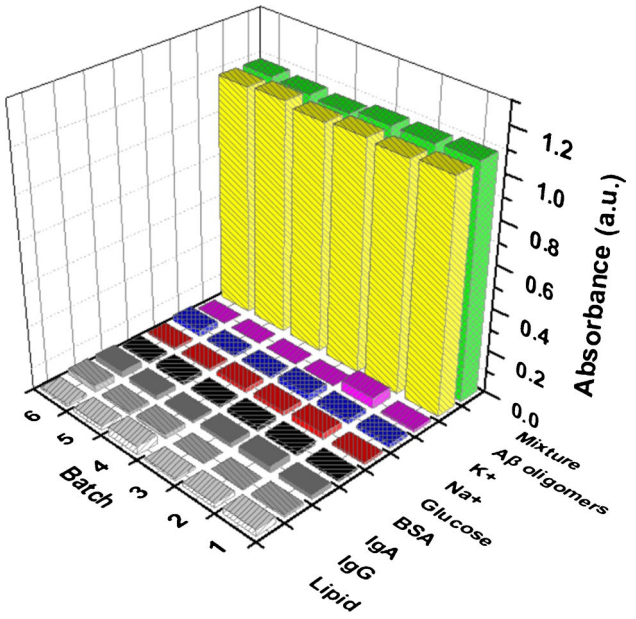

Fig. 4 The selectivity of the proposed optical biosensor

Properties of the optical biosensor

The quantitative detection of AβO is accomplished using an optical biosensor based on absorbance at 650 nm. As demonstrated in Fig. 5a, the absorption peak at 650 nm gradually increases with the increase in target (AβO) concentration (0.0001–10 nM). The correlation coefficient, calculated as y=0.0797 ln(x) + 0.8898, is 0.9936 (Fig. 5b). The limit of detection is evaluated to be 0.03 pM under a signal-to-noise

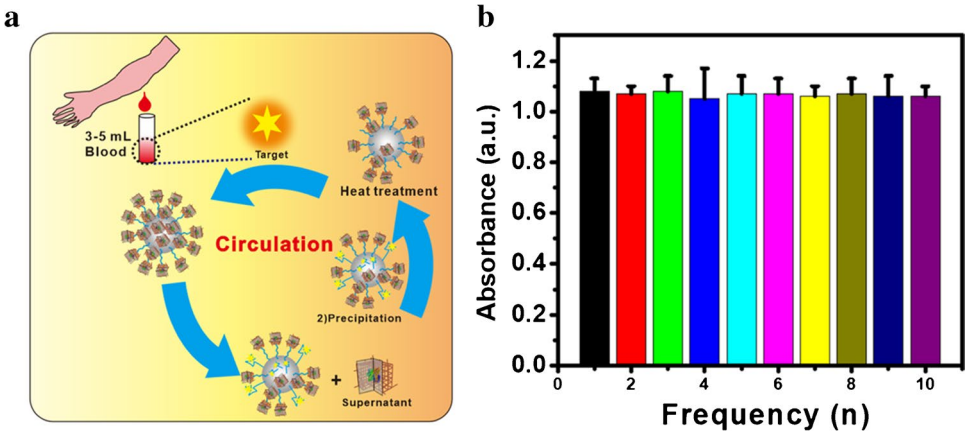

Fig. 3 (**a**) Mechanism of optical biosensor reuse, and (**b**) reusability investigated by comparison of the absorbance of UV–Vis for Apt-Fe_3O_4 with 10 nM AβO

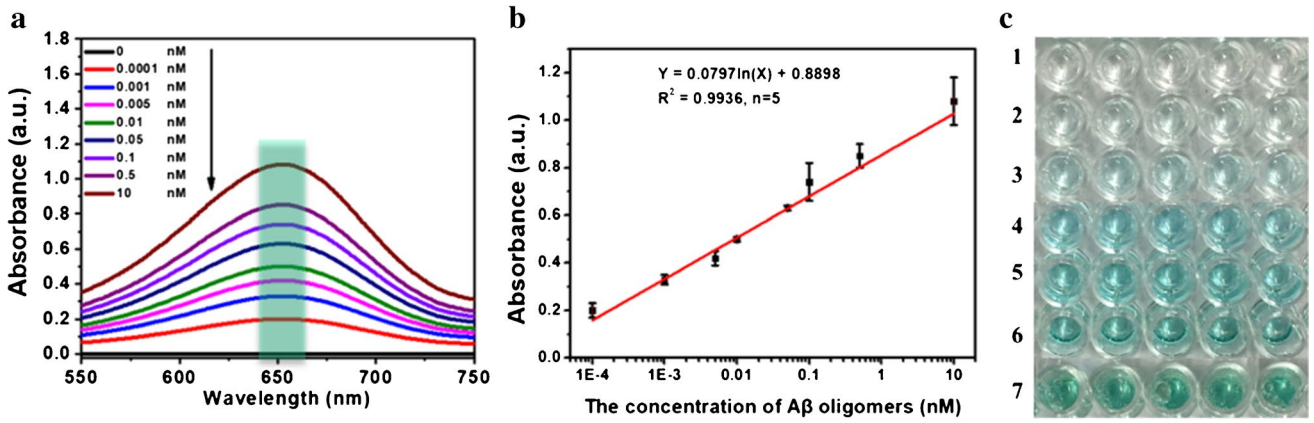

Fig. 5 (**a**) UV–Vis spectra of the developed optical biosensor with various concentrations of AβO. (**b**) The standard curve of the absorbance peak with various concentrations of AβO in 650 nm. (**c**) The color optical map with various concentrations of AβO. The numbers 1 to 7 represent the different concentrations of AβO (0, 0.001, 0.01, 0.1, 0.5, 1, and 10 nM, respectively)

Table 1 The current detection methods for AβO, the linear range, and limit of detection (LOD)

Methods	Linear range	LOD	Storage temperature	Reference
Fluorescence	20 nM–10 μM	12.5 nM	-	[30]
Fluorescence	0.025 pM–25 nM	10 fM	4 °C	[19]
Immunoassay	0.02 nM–25 nM	50 pM	4 °C	[31]
SERS	100 pM–740 pM	70 pM	-	[32]
Electrochemiluminescence	0.1 pM–10 pM	71 fM	4 °C	[33]
This method	0.1 pM–10 nM	0.03 pM	37 °C	This work

The symbol '-' indicates that the storage temperature could not be determined for the corresponding assay. *SERS* surface-enhanced Raman spectroscopy

(S/N) ratio of 3. The reproducibility of the optical biosensor is measured by the repeated detection of 10 nM AβO five times. The results of the analysis demonstrate an excellent relative standard deviation (RSD) of 2.95%. As displayed in Fig. 5c, the color development under different concentrations of AβO normal saline solution can be distinguished with the naked eye.

This method is compared with other assay methods for AβO detection in Table 1. The results show that the optical biosensor can be applied for the measurement of AβO in practical samples over a wide range of concentrations. Another advantage of the optical biosensor is that it can be stored at high temperature (37 °C) with high activity (Table 1 and Fig. 2c). Therefore, the heat instability of biosensors will be resolved by the development of optical biosensors.

Analytical application

To establish the reliability and feasibility of this method for clinical application, the AβO in blood samples was measured. The accuracy of AβO detection in serum samples was also estimated by monitoring the recovery of AβO using the standard addition method. The measurement results for AβO in blood serum obtained using the developed method were compared with a commercial ELISA kit. As shown in Table 2, the optical biosensor demonstrated good accuracy for the proposed method for detection of AβO. Additionally, the results for the optical biosensor were coherent with the results of the ELISA kit.

Table 2 Recovery results for AβO obtained via the developed assay and commercial ELISA kit ($\bar{x}\pm s$, $n=6$)

Sample	Background (nM)	Added concentration (nM)	ELISA (nM)	Developed assay (nM)	Recovery (%)
1	0	0.010	0.010±0.011	0.009±0.001	90.0
2	0	0.100	0.096±0.021	0.095±0.018	95.0
3	0	0.500	0.48±0.05	0.490±0.101	98.00
4	0	1.000	0.98±0.05	1.01±0.050	101.00
5	0	5.000	4.99±0.250	4.98±0.150	99.60

Conclusion

A novel and thermostable biosensor was developed through the application of biomimetic mineralization HRP@Fe-MOF as signal probe. Compared with existing assays for measuring AβO, the new approach offers superior stability, sensitivity, specificity, and long-term maintenance of high activity at 37 °C. Meanwhile, the Fe(II)-based MOF-armored HRP hopefully solves the thermal instability of the biosensor. Moreover, this approach was successful applied for AβO measurement in blood serum samples. The results suggest that this biosensor has great promise for improving the detection of AβO to enable the early diagnosis and appropriate therapeutic options for patients with AD.

Supplementary Information The online version contains supplementary material available at https://doi.org/10.1007/s00216-022-04367-y.

Author contribution All authors have accepted responsibility for the entire content of this manuscript and approved its submission.

Funding This work was financially supported by the 2018 Academic New Seedling Cultivation and Innovation Exploration Project of Guizhou Provincial Science and Technology Department (No. [2018]5784-05) and Ph. D. Foundation of Zunyi Normal College (No. BS[2019]10).

Declarations

Ethics approval The study was approved by the Ethics Committee of Ningbo No. 7 Hospital.

Conflict of interest The authors declare no competing interests.

Source of biological material Serum sample were collected in the Department of Laboratory Medicine of Ningbo No. 7 Hospital.

Statement on animal welfare Not applicable.

References

1. Vicente-Zurdo D, Romero-Sánchez I, Rosales-Conrado N, León-González ME, Madrid Y. Ability of selenium species to inhibit metal-induced Aβ aggregation involved in the development of Alzheimer's disease. Anal Bioanal Chem. 2020;412(24):6485–97.
2. Agami M, Shaalan RA, Belal SF, Ragab MA. LC-MS bioanalysis of targeted nasal galantamine bound chitosan nanoparticles in rats' brain homogenate and plasma. Anal Bioanal Chem. 2021;413(20):5181–91.
3. Viola KL, Klein WL. Amyloid β oligomers in Alzheimer's disease pathogenesis, treatment, and diagnosis. Acta Neuropathol. 2015;129(2):183–206.
4. Mars A, Hamami M, Bechnak L, Patra D, Raouafi N. Curcumin-graphene quantum dots for dual mode sensing platform: electrochemical and fluorescence detection of $APOe_4$, responsible of Alzheimer's disease. Anal Chim Acta. 2018;1036:141–6.
5. Gaetani L, Höglund K, Parnetti L, Pujol-Calderon F, Becker B, Eusebi P, et al. A new enzyme-linked immunosorbent assay for neurofilament light in cerebrospinal fluid: analytical validation and clinical evaluation. Alzheimers Res Ther. 2018;10(1):1–13.
6. Ma H, Liu S, Liu Y, Zhu J, Han XX, Ozaki Y, et al. In-situ fingerprinting phosphorylated proteins via surface-enhanced Raman spectroscopy: single-site discrimination of tau biomarkers in Alzheimer's disease. Biosens Bioelectron. 2021;171:112748.
7. Caratelli V, Ciampaglia A, Guiducci J, Sancesario G, Moscone D, Arduini F. Precision medicine in Alzheimer's disease: an origami paper-based electrochemical device for cholinesterase inhibitors. Biosens Bioelectron. 2020;165:112411.
8. Guo Q, Yang J, Zhao J, Zhang J, Yuan R, Chen S. A novel aptamer biosensor based on polydopamine quenched electrochemiluminescence of polyfluorene nanoparticles for amyloid-β oligomers detection. Sens Actuators B Chem. 2022;368:132204.
9. Saerens D, Huang L, Bonroy K, Muyldermans S. Antibody fragments as probe in biosensor development. Sensors. 2008;8(8):4669–86.
10. Ma C, Feng S, Zhou J, Chen R, Wei Y, Liu H, et al. Enhancement of H_2O_2 decomposition efficiency by the co-catalytic effect of iron phosphide on the Fenton reaction for the degradation of methylene blue. Appl Catal B. 2019;259:118015.
11. Hu Z, Yin Y, Liu Q, Zheng X. A functional FePt@ MOFs (MIL-101 (Fe)) nano-platform for high efficient colorimetric determination of H_2O_2. Analyst. 2019;144(8):2716–24.
12. Kou X, Tong L, Shen Y, Zhu W, Yin L, Huang S, et al. Smartphone-assisted robust enzymes@MOFs-based paper biosensor for point-of-care detection. Biosens Bioelectron. 2020;156:112095.
13. Sheta SM, El-Sheikh SM, Abd-Elzaher MM. A novel optical approach for determination of prolactin based on Pr-MOF nanofibers. Anal Bioanal Chem. 2019;411(7):1339–49.
14. Li J, Ma M, Zhang C, Lu R, Zhang L, Zhang W. Synthesis of a molecularly imprinted polymer using MOF-74 (Ni) as matrix for selective recognition of lysozyme. Anal Bioanal Chem. 2020;412(26):7227–36.
15. Yi X, Dong W, Zhang X, Xie J, Huang Y. MIL-53 (Fe) MOF-mediated catalytic chemiluminescence for sensitive detection of glucose. Anal Bioanal Chem. 2016;408(30):8805–12.
16. Wang N, Wu Y, Wang M, Li Z, Wang G, Su X. Design of a dual-signal sensing platform for d-penicillamine based on UiO-66-NH_2 MOFs and APBA@ alizarin red. Analyst. 2021;146(17):5280–6.
17. Wan H, Cao X, Liu M, Zhang F, Sun C, Xia J, et al. Aptamer and bifunctional enzyme co-functionalized MOF-derived porous carbon for low-background electrochemical aptasensing. Anal Bioanal Chem. 2021;413(25):6303–12.
18. Miao YB, Pan WY, Chen KH, Wei HJ, Mi FL, Lu MY, et al. Engineering a nanoscale Al-MOF-armored antigen carried by a "trojan horse"-like platform for oral vaccination to induce potent and long-lasting immunity. Adv Funct Mater. 2019;29(43):1904828.
19. Ren HX, Zhong Q, Miao YB, Wen XW, Wu GY, Wang HL, et al. A label-free reusable aptasensor for Alzheimer's disease. Microchim Acta. 2020;187(9):1–8.
20. Liu Y, Purich DL, Wu C, Wu Y, Chen T, Cui C, et al. Ionic functionalization of hydrophobic colloidal nanoparticles to form ionic nanoparticles with enzymelike properties. J Am Chem Soc. 2015;137(47):14952–8.
21. Liang X, Wang X, Zhuang J, Chen Y, Wang D, Li Y. Synthesis of nearly monodisperse iron oxide and oxyhydroxide nanocrystals. Adv Funct Mater. 2006;16(14):1805–13.
22. Zhang Y, Ren HX, Miao YB. Visualization and colorimetric determination of clenbuterol in pork by using magnetic beads modified with aptamer and complementary DNA as capture probes, and G-quadruplex/hemin and DNA antibody on the metal-organic framework MIL-101 (Fe) acting as a peroxidase mimic. Microchim Acta. 2019;186(8):1–8.

23. Wang X, Hyun JL, Ahjeong S. Characterization of denaturation and renaturation of DNA for DNA hybridization. Environ Health Toxicol. 2014;29:e2014007.
24. Nguyen VH, Nguyen TD, Bach LG, Hoang T, Bui QTP, Tran LD, et al. Effective photocatalytic activity of mixed Ni/Fe-base metal-organic framework under a compact fluorescent daylight lamp. Catalysts. 2018;8(11):487.
25. Deng Z, Jin W, Yin Q, Huang J, Huang Z, Fu H, et al. Ultrasensitive visual detection of Hg^{2+} ions via the Tyndall effect of gold nanoparticles. Chem Comm. 2021;57(21):2613–6.
26. Larson NR, Wei Y, Middaugh CR. Label-free, direct measurement of protein concentrations in turbid solutions with a UV–visible integrating cavity absorbance spectrometer. Anal Chem. 2018;90(8):4982–6.
27. Gong C, Gong Y, Oo MKK, Wu Y, Rao Y, Tan X, et al. Sensitive sulfide ion detection by optofluidic catalytic laser using horseradish peroxidase (HRP) enzyme. Biosens Bioelectron. 2017;96:351–7.
28. Ma Y, Geng F, Wang Y, Xu M, Shao C, Qu P, et al. Novel strategy to improve the sensing performances of split ATP aptamer based fluorescent indicator displacement assay through enhanced molecular recognition. Biosens Bioelectron. 2019;134:36–41.
29. Basu D, Kulkarni R. Overview of blood components and their preparation. Indian J Anaesth. 2014;58(5):529.
30. Liu L, Chang Y, Yu J, Jiang M, Xia N. Two-in-one polydopamine nanospheres for fluorescent determination of beta-amyloid oligomers and inhibition of beta-amyloid aggregation. Sens Actuators B Chem. 2017;251:359–65.
31. Zhao J, Chang W, Liu L, Xing X, Zhang C, Meng H, et al. Graphene oxide-gold nanoparticle-aptamer complexed probe for detecting amyloid beta oligomer by ELISA-based immunoassay. J Immunol Methods. 2021;489:112942.
32. Zhou Y, Liu J, Zheng T, Tian Y. Label-free SERS strategy for in situ monitoring and real-time imaging of Aβ aggregation process in live neurons and brain tissues. Anal Chem. 2020;92(8):5910–20.
33. Yin L, Wang Y, Tan R, Li H, Tu Y. Determination of β-amyloid oligomer using electrochemiluminescent aptasensor with signal enhancement by AuNP/MOF nanocomposite. Microchim Acta. 2021;188(2):1–8.